Research Article J. Electrochem. Sci. Technol., 2024, 15(4), 512-520

Surface Nitridation of Nano-sized Anatase TiO_2 using Urea and Thiourea for Enhanced Electrochemical Performance in Lithium-ion Batteries

Wonyoung Song[1], Oh B. Chae[1]*, and Ji Heon Ryu[2]*

[1]School of Chemical, Biological and Battery Engineering, Gachon University, Seongnam-si, Gyeonggi-do 13120, Republic of Korea
[2]Graduate School of Convergence Technology and Energy, Tech University of Korea, Siheung-si, Gyeonggi-do, Republic of Korea

ABSTRACT

Given the critical importance of safety in lithium-ion batteries (LIBs), titanium dioxide (TiO_2) is widely regarded as a reliable material for the negative electrode. Anatase TiO_2 is a safe negative electrode material in LIBs, attributed to its high redox potential (1.5–1.8 V vs. Li/Li^+), which exceeds that of commercially available graphite, alleviating the risk of lithium plating. In addition, TiO_2 has gained considerable attention as a cost-effective negative electrode material for LIBs, owing to its versatility in nano-sized forms. The use of nano-sized TiO_2 as an electrode-active material reduces the diffusion distance of Li^+ ions. However, TiO_2 is adversely affected by its inherently low electronic conductivity, which hinders its rate performance. Herein, we investigated the surface treatment of commercially available TiO_2 nanoparticles with anatase structure using a heat-treatment process in the presence of urea or thiourea. Our objective was to leverage the eco-friendly nitridation of TiO_2 from the thermal decomposition of urea or thiourea, enhancing their electrochemical performance in lithium-ion batteries while minimizing environmental impact. Specifically, we employed an autogenic reactor (AGR) in a closed space to ensure an adequate reaction between NH_3 and TiO_2, preventing NH_3 from escaping into the external environment, as observed in open systems. Consequently, surface nitridation enhanced the overall electrochemical performance, including the rate capability, capacity retention, and initial Coulombic efficiency (ICE). Notably, a remarkable enhancement was observed for the thiourea-treated TiO_2. Compared to the pristine TiO_2, the thiourea-treated TiO_2 demonstrated a nearly threefold increase in capacity at 1.0 C and a nearly two-fold increase in capacity retention.

Keywords : TiO_2 nanoparticles, Negative electrode, Surface nitridation, Urea, Lithium-ion batteries

Received : 2 May 2024, Accepted : 30 May 2024

1. Introduction

Lithium-ion batteries (LIBs) have exhibited a significant surge in demand across various fields owing to their efficient energy storage capabilities and convenient usability. Additionally, owing to their inherent advantages, including high specific capacity and voltage, low self-discharge, and the absence of memory effects, LIBs demonstrate superior performance over any preceding battery systems [1–3]. However, recent incidents such as fires and explosions have underscored the safety concerns with LIBs, making them a pressing challenge. Consequently, the constrained safety performance of LIBs impedes their market expansion. Lithium plating on the negative electrodes is a significant issue affecting the safety of LIBs. The conventional graphite anode undergoes lithium plating owing to the proximity of the lithium insertion potential (0.1 vs. Li/Li^+) to the deposition potential of lithium metal [4–6]. Excessive Li deposition can lead to the formation of dendrites, which can result in internally short-circuit the cell. To effectively mitigate the risks associated with lithium plating, it is imperative to develop negative electrode materials that exhibit higher lithiation potentials.

Transition metal oxides (TMOs) have been extensively studied as alternative materials to replace commercially used graphite [7–11]. TMOs can be

*E-mail address: obchae@gachon.ac.kr (O. B. Chae)
ryujh@tukorea.ac.kr (J. H. Ryu)

DOI: https://doi.org/10.33961/jecst.2024.00465

broadly categorized into two groups based on their reactivity with lithium: conversion and insertion types. Among them, insertion-type TMOs are characterized by stronger metal–oxygen bonding than conversion-type TMOs. This robust bonding ensures that during lithiation the metal–oxygen bonds remain intact, allowing Li^+ ions to permeate into the lithium storage sites within the structure of metal oxides and engage in the reaction ($MO + xLi^+ + xe^- \rightarrow Li_xMO$) [7,8,11–13]. Insertion-type TMOs, although relatively lower in capacity than conversion-type TMOs, exhibit superior cycling performance owing to their smaller volume changes (<3%) during lithiation/delithiation cycles. Insertion-type TMOs include TiO_2, $Li_4Ti_5O_{12}$, V_2O_5, and MoO_2. Among these, titanium dioxide (TiO_2) exists in various phases such as anatase [13–17], rutile [18,19], TiO_2(B) [20,21], and brookite [22,23]. Research efforts have predominantly focused on investigating the anatase phase, which exhibits the best performance for lithium-ion storage owing to its inherently stable crystal structure. Furthermore, anatase TiO_2 has gained attention as a safe negative electrode material for LIBs because of its higher operating potential (>1.5 V vs. Li/Li^+) than that of carbonaceous negative electrode materials, which minimizes lithium plating issues. This elevated reaction potential prevents the reduction of the electrolyte and the formation of a solid electrolyte interphase (SEI) on the electrode surface [24,25]. Anatase TiO_2 is characterized by a three-dimensional network formed by the stacking of one-dimensional zigzag chains of TiO_6 octahedra through distorted edge-sharing (space group $I4_1/amd$). This stacking process results in the formation of vacant zigzag channels within the anatase framework, facilitating the insertion of Li^+ ions into these octahedral sites. The majority of anatase TiO_2 materials utilize only half of their capacity through the insertion reaction of Li^+ ions ($TiO_2 + xLi^+ + xe^- \rightarrow Li_xTiO_2$), wherein half a Li^+ ion is inserted per TiO_2 molecule [26]. Given the high working potential previously mentioned, nano-sized TiO_2 with a large surface area has a relatively minor decline in reversible capacity owing to less electrolyte decomposition. However, owing to its low electronic conductivity (~10^{-12} S cm^{-1}), anatase TiO_2 tends to exhibit poor rate characteristics [27]. To enable fast charging, it is imperative to enhance the electronic conductivity of anatase TiO_2.

To enhance electron transport, various methods have been developed, including hybridization with highly conductive materials and the introduction of anion dopants [17,28–31]. Surface treatment of anatase TiO_2 is a prominent approach widely employed to improve its rate characteristics because of its inherently poor electronic conductivity [32]. Anion dopants including N [33–37], S [28,38], C [39–41], F [21,42], and B [31,43] have been introduced into TiO_2 lattice to mitigate the electron transport resistance. Among them, N dopants, which have been extensively researched in the field of photocatalysis, exhibit a predominant tendency to be located on the surface layer of TiO_2. This behavior can be attributed to the higher energy level exhibited by the surface relative to the bulk and the poor solubility of the dopants [44,45]. The surface of N-doped TiO_2 can be transformed into TiN or $TiO_{2-x}N_x$ through heat treatment in NH_3 gas. This modification significantly enhances the electrochemical performance of the TiO_2 electrode by introducing an electrically conductive phase on the surface [46,47]. However, the use of corrosive and toxic NH_3 gas hinders their commercial application. Therefore, research on less-toxic alternatives capable of improving the poor electronic conductivity of TiO_2 is imperative [48,49].

In this study, we investigated the surface nitridation of TiO_2 via the thermal decomposition of urea (NH_2CONH_2) in an autogenic reactor (AGR) in a closed reaction environment. Additionally, for the synergistic effects of N and S, thiourea (NH_2CSNH_2) was introduced. The thermal decomposition of thiourea was conducted under an inert atmosphere. Urea decomposes below 200°C and generates NH_3 gas [50]. Similarly, thiourea decomposes at 180–220°C, releasing gases including NH_3 and H_2S [51]. Therefore, both substances can serve as coating materials for AGR-based treatments designed to facilitate nitridation at temperatures above 700°C [52]. This method is simple and applicable to mass production. Surface-nitridated TiO_2 demonstrated enhanced electrochemical performance compared to that of pristine TiO_2. In particular, the thiourea-treated sample exhibited excellent rate capability across all current densities. The thiourea-treated sample exhibited a nearly threefold increase in capacity compared to the pristine sample at 1.0 C and demonstrated nearly double the capacity retention.

2. Experimental

2.1 Material synthesis

Nano-sized anatase TiO_2 powder was purchased from Daejung Chemicals & Metals Co.Ltd. After homogeneous mixing of TiO_2 and 30 wt% urea or thiourea using a pestle and mortar, the mixture was placed in an autogenic reactor (AGR, 316 stainless steel, Swagelok), and the AGR was isolated from the air atmosphere by closing the cap. The AGR was heated to 700°C for 10 minutes with a heating and cooling rate of 10°C min^{-1} in the electric muffle furnace. The synthesized powder was obtained after disassembling the AGR.

2.2 Cell preparation for electrochemical tests

Composite electrodes consisting of pristine TiO_2 and surface-nitridated TiO_2 were uniformly mixed with poly(vinylidene fluoride) (PVDF, KF1100), carbon black (super-P, Timcal), and anhydrous N-methyl-2-pyrrolidone (NMP, Aldrich) as a solvent. The weight ratios of active material, polymeric binder, and carbon black was employed for the electrode compositions of 80:10:10. The resulting slurry was then cast on copper foil to a thickness of approximately 20 μm. The composite electrode was thoroughly dried in a convection oven at 120°C to remove the NMP solvent. The electrode mass loading was adjusted to about 2.5 ± 0.5 mg cm^{-2}. To enhance the interparticle connectivity and maintain electrical conductivity, a roll press was employed. Subsequently, electrodes with a diameter of 11 mm were prepared using a punching machine. These electrodes were assembled into 2032-type coin cells, along with a separator (polypropylene, Celgard), lithium metal counter electrode, and an electrolyte comprising 1.3 M $LiPF_6$ in a 3:7 vol% mixture of ethylene carbonate (EC) and ethyl methyl carbonate (EMC) (Panaxetec, battery grade).

2.3 Electrochemical measurements

A WBCS-3000 cycler (Wonatech) was used to conduct galvanostatic charge/discharge tests and rate capability evaluations. In galvanostatic cycling tests, the Li/TiO_2 cells were cycled under a constant current density of 15 mA g^{-1} (approximately 0.1 C current) within the voltage ranges of 1.0–2.5 V (vs. Li/Li^+). Various current conditions were applied for the rate capability measurements: 0.1, 0.2, 0.5, and 1.0 C.

2.4 Materials characterization

Scanning electron microscopy (SEM) was performed using a JEOL instrument (Tokyo, Japan). The particle size distribution of each sample was determined by analyzing the SEM images using ImageJ software. X-ray diffraction (XRD) analyses were performed using a Bruker D8 Advance with Cu·Kα radiation (wavelength = 1.5418 Å). The measurements were performed over the 2θ range from 20° to 70° at a scan rate of 5° min^{-1}.

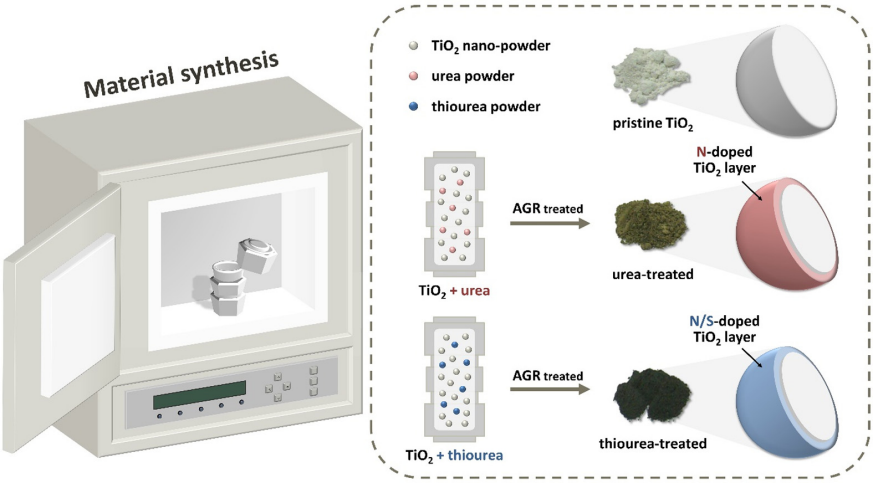

Fig. 1. Schematic of the preparation process of surface-nitridated TiO_2 in one-step surface nitridation by thermal decomposition of urea and thiourea, respectively.

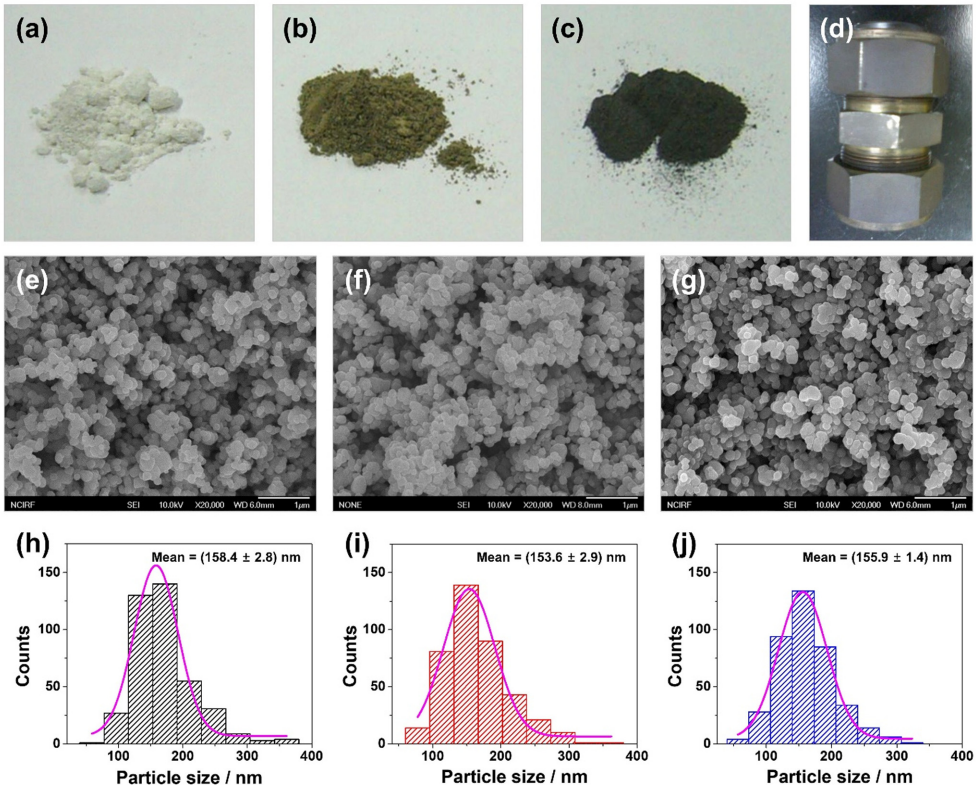

Fig. 2. Pictures, SEM images, and particle size distribution of (a,e,h) pristine TiO_2 and surface-nitridated TiO_2 using (b,f,i) urea and (c,g,j) thiourea, respectively. (d) Autogenic reactor used in the nitridation of the TiO_2 surface.

3. Results and Discussion

The experiment was conducted using an autogenic reactor (AGR), as shown in Fig. 1. The AGR is designed to establish and sustain high-pressure and high-temperature conditions within a confined space, which is essential for the synthesis of various materials. These extreme conditions provide controlled environments for the formation and transformation of materials. The AGR treatment enables the generation of highly electrically conductive materials through pyrolysis reactions at elevated temperatures and pressures. In addition, the AGR process is relatively simple, facilitating scalability from laboratory-scale experiments to industrial production and ensuring the production of materials in quantities suitable for commercial applications [48,49].

Fig. 2 shows the alterations in powder colors and particle shapes in response to urea or thiourea through powder images and SEM images. In Fig. 2a–c, the pristine TiO_2 powder is white, whereas the surface-nitridated TiO_2 powder displays a different color in its synthesized form. Urea treatment results in a dark yellow color [53], whereas thiourea treatment yields an even darker hue [54]. Considering that the color of each powder was uniform, the synthesis was performed well overall. SEM analyses (Fig. 2e–g) were conducted to investigate the surface morphology after AGR treatment. The pristine TiO_2 powder exhibits a spherical morphology, as observed in the SEM image (Fig. 2e). The SEM images of the surface-nitridated samples (Fig. 2f,g) indicate no significant changes in both morphology and particle size after heat treatment. Additionally, the particle size distribution for the samples was determined using ImageJ software (Fig. 2h–j). For each sample, a measurement of 400 particles was conducted, wherein the diameter of each particle was measured. The pristine TiO_2 powder exhibits an average particle size of 158.4 ± 2.8 nm (Fig. 2h). For the urea-treated sample, the average particle size was measured to be 153.6 ± 2.9 nm, and for the thiourea-treated sample, it was

155.9 ± 1.4 nm (Fig. 2i,j). The constancy in particle size and shape suggests that these variables do not influence performance. Consequently, the performance is determined solely by the material used for surface modification. Meanwhile, surface-nitridated TiO_2 powder is expected to exhibit a uniform distribution of N and S elements. This is based on previous studies that demonstrated a homogeneous distribution of Ti, O, N, and S elements in nitridated TiO_2 [55,56].

The alterations in the powder color prompted an investigation into the crystal structures of the materials after surface treatment with urea or thiourea. Fig. 3 shows the XRD patterns of the pristine, urea-treated, and thiourea-treated TiO_2 samples. The XRD pattern for pristine TiO_2 (Fig. 3a) exhibits seven distinct peaks at $2\theta = 25.13^o$, 37.63^o, 47.88^o, 53.73^o, 54.92^o, 62.71^o, and 68.64^o, corresponding to (1 0 1), (0 0 4), (2 0 0), (1 0 5), (2 1 1), (2 0 4), and (1 1 6) crystal planes, respectively. These peaks aligned with the tetragonal crystal planes of anatase TiO_2, which is consistent with the standard spectrum (JCPDS no.: 21-1272). Notably, there is no evidence of other crystalline phases, such as rutile and brookite. The XRD patterns of surface-nitridated TiO_2 (Fig. 3b,c) exhibit no discernible differences in the bulk structure, indicating that the AGR heat treatment method selectively modifies the surface without altering the crystal structure of the mother phase. That is, no deformation of TiO_2 occurs after the AGR heat-treatment process. The crystallite size of each particle is calculated by applying the full-width half-maximum (FWHM) values of the (1 0 1) main peaks in Fig. 3 to Scherrer's equation ($D = K\lambda/\beta\cos\theta$). The particle sizes of pristine and surface-nitridated TiO_2 were determined to be in the range of 46–63 nm based on the equation. The consistent crystallite sizes suggest similar crystallinities for all three samples. However, the diffraction peaks of compounds containing nitrogen or sulfur were not evident in the XRD pattern, likely because of their minimal presence in the total powder composition. Additionally, the substitution of O^{2-} by N^{3-} and S^{2-} during AGR treatment resulted in peaks appearing at the same positions, contributing to the lack of significant differences in the XRD pattern [56]. Furthermore, previous studies established that

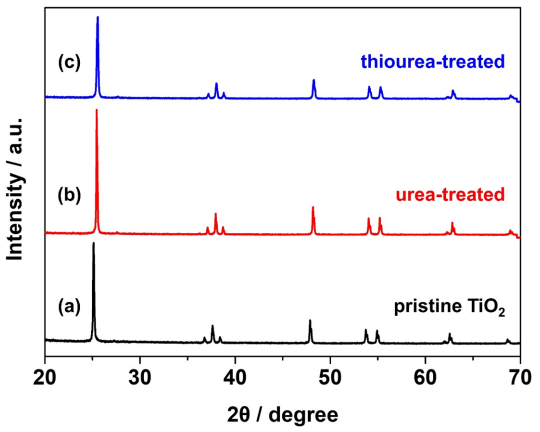

Fig. 3. XRD patterns of (a) pristine TiO_2, (b) urea-treated TiO_2, and (c) thiourea-treated TiO_2 samples.

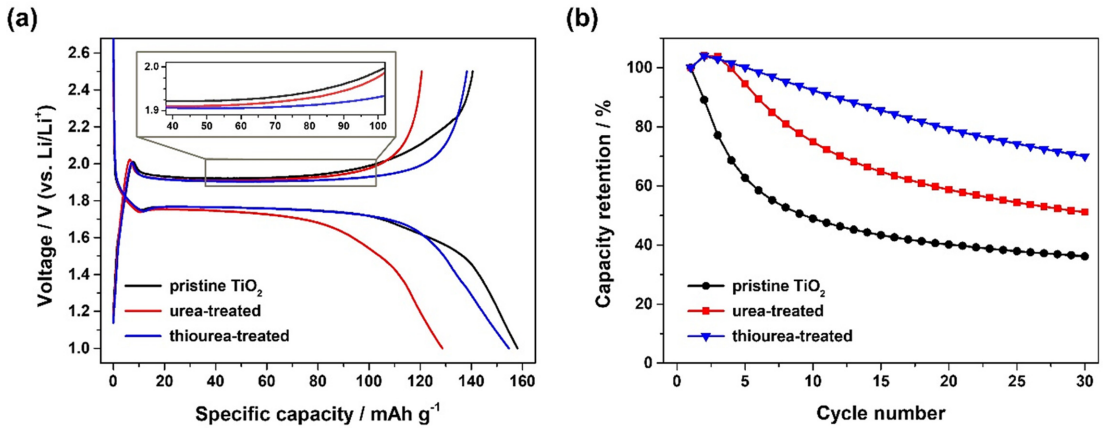

Fig. 4. (a) Voltage profiles at 1st cycle and (b) capacity retention of Li/TiO_2 half cells comprising pristine, urea-treated, and thiourea-treated TiO_2 samples.

TiO_2 annealed in the presence of urea or thiourea exhibits the substitution of N for O sites, thereby resulting in the formation of a Ti–N layer on the TiO_2 surface [49,56,57]. The absence of heterogeneous XRD peaks indicates that the nitridation process predominantly affected the surface.

Fig. 4a presents the initial voltage profiles and the capacity retention for pristine, urea-treated, and thiourea-treated TiO_2. The galvanostatic charge/discharge test was conducted over a voltage range of 1.0–2.5 V at a rate of 0.1 C. The three types of TiO_2 exhibited typical voltage profiles of an anatase TiO_2 negative electrode [58]. All three samples displayed a lithiation (discharge) plateau observed at ~1.76 V and a region of voltage drop to cut-off 1.0 V. The delithiation (charge) plateau starts at ~1.9 V. These potentials align with those reported in previous studies (~1.75 and ~1.88 V, respectively) [59,60]. A magnification of the voltage profile provides additional insights into internal resistance. A detailed analysis of the 1.9–2.0 V range revealed that the overpotential decreased in the order of pristine, urea-treated, and thiourea-treated TiO_2. This suggests that internal resistance also decreased in the same sequence. These analytical results demonstrate that the surface-treatment process in this study effectively enhances the electronic conductivity of the samples by doping N or S onto the surface. Consequently, the reduced internal resistance of surface-nitridated TiO_2 is expected to improve both cycle performance and rate capability. The electrochemical performance of our samples was comparable to that reported in previous studies [14,58]. The pristine TiO_2 exhibited 158.03 mAh g^{-1} (lithiation), 140.53 mAh g^{-1} (delithiation), during the first cycle. The lithiation capacity of pristine TiO_2 was close to its theoretical capacity (168 mAh g^{-1}, 0.5 mol of Li). The first-cycle lithiation and delithiation capacities were 128.64, 120.60 mAh g^{-1} for urea-treated TiO_2, and 154.68, 138.23 mAh g^{-1} for thiourea-treated TiO_2, respectively. This demonstrates that for the surface-nitridated samples, the irreversible capacity was smaller during the first-cycle lithiation/delithiation than that of the pristine counterpart. Additionally, the initial Coulombic efficiency (ICE) of the surface-nitridated samples improved compared to that of the pristine sample. Fig. 4b shows the reversibility of the electrochemical reactions of the three samples over 30 lithiation/delithiation cycles at a 0.1 C-rate. The capacity retention rates for each sample after 30 cycles were 36.15%, 51.11%, and 70.01% for pristine, urea-treated, and thiourea-treated samples, respectively. The capacity of the cells with the pristine TiO_2 electrode experienced sharp degradation within the first 10 cycles. Conversely, the surface-nitridated samples exhibited superior capacity retention compared to their pristine counterparts. In particular, the cycling performance of the cell with the thiourea-treated TiO_2 electrode demonstrated the most significant improvement, nearly doubling the capacity retention of the pristine TiO_2 electrode.

Rate capability tests of the three samples were conducted to investigate the power densities, as shown in Fig. 5. Thiourea-treated TiO_2 exhibited higher reversible capacities than the other samples at all the current densities tested. At the low C-rate (0.1 C, 1st cycle), the sample heat treated in the AGR with urea (119.32 mAh g^{-1}) showed lower specific capacities than the pristine TiO_2 (133.82 mAh g^{-1}). However, from 0.1 C (2nd cycle) onward, all surface-nitridated samples demonstrated higher specific capacities than the pristine sample. This improved rate capability of the surface-nitridated TiO_2 can be confirmed by comparing the cycle performance at high C-rates (≥0.2 C-rate). At current densities of 0.2 C, 0.5 C, and 1.0 C, the urea-treated sample exhibited approximately 1.2, 1.3, and 1.5 times higher specific capacities compared to the pristine sample, respectively. The thiourea-treated sample demonstrated approximately 1.5, 2.0, and 3.0 times higher specific capacities than the pristine sample at the respective current densi-

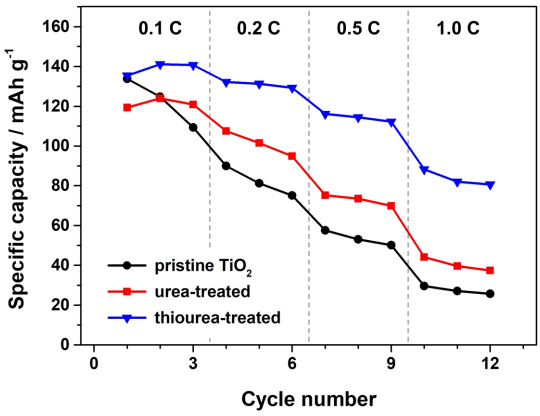

Fig. 5. Rate capabilities of the coin half cells comprising pristine, urea-treated, and thiourea-treated TiO_2 samples.

ties. Note that the capacity ratio between 0.1 C and 1.0 C of pristine, urea-treated, and thiourea-treated TiO_2 were 22.1%, 37.0%, and 65.1%, respectively. These results indicate that the thiourea-treated sample exhibited the most improved rate capabilities compared to other samples across all current densities, notably achieving an approximately threefold improvement in capacity at 1.0 C compared to pristine TiO_2.

Previous studies have yielded valuable insights into the outstanding electrochemical performance of the thiourea-treated TiO_2 sample compared with that of the urea-treated sample. This can be attributed to the following two factors. The first reason appears to be that the band gap of N/S–TiO_2 is narrower than that of N–TiO_2. Viswanath et al. [61] reported a considerable reduction in the band gap of N/S–TiO_2 (0.22 eV reduction) compared to that of N–TiO_2 (0.11 eV reduction). This reduction underscores the inevitable enhancement of the electronic conductivity in N/S–TiO_2 compared to that in N–TiO_2. The second reason is the reduction in resistance resulting from improved electronic conductivity. As reported by Jiao et al. [62], in the case of N/S–TiO_2 (by NH_3 and H_2S gases), a substantial decrease was noted in both the ohmic resistance (R_e) and charge-transfer resistance (R_{ct}) compared to N–TiO_2 (by NH_3 gas). Compared to pristine, N–TiO_2 exhibited a reduction of 18.2% in R_e and 35.6% in R_{ct}. By contrast, N/S–TiO_2 showed more substantial reductions, with a 31.4% reduction in R_e and a 68.2% reduction in R_{ct} relative to the pristine TiO_2. For these two reasons, surface-nitridated TiO_2 demonstrates enhanced electrochemical performance compared to pristine TiO_2. Among the surface-nitridated TiO_2 samples, the thiourea-treated sample exhibits the highest rate capability and capacity retention.

4. Conclusions

In this study, to enhance the transport of electrons, we applied the surface nitridation of TiO_2 through the thermal decomposition of urea or thiourea. The thermal decomposition was conducted in an AGR at 700°C for a closed reaction environment. Facilitated by the AGR, the reaction between TiO_2 and urea induces surface nitridation, consequently enhancing the electronic conductivity and thereby improving the electrochemical performance. Furthermore, substituting urea with thiourea promoted surface nitridation owing to the synergistic effect arising from the coexistence of both N and S, resulting in further enhanced electrochemical performance. In terms of capacity retention, thiourea-treated TiO_2 exhibited a nearly two-fold improvement over pristine TiO_2. Moreover, the thiourea-treated sample exhibited superior rate performance across all current densities, particularly at 1.0 C where the capacity demonstrated an approximately threefold increase compared to that of the pristine sample. These enhanced performance outcomes are attributed to the improvement in the electronic conductivity of the samples through the AGR treatment, with the use of thiourea notably enhancing the electronic conductivity more than when using urea. Compared to the other samples, the thiourea-treated TiO_2 demonstrated the narrowest band gap, thereby exhibiting the highest electronic conductivity. This leads to lower resistance, resulting in superior electrochemical performance, including rate capability and capacity retention. In the context of this study, a one-step surface-nitridation process was employed, which avoided the use of toxic NH_3 and H_2S gases, making it particularly suitable for large-scale production. This observation strengthens the potential of TiO_2 as a versatile material for energy storage given its enhanced safety and excellent performance.

Acknowledgements

This research was supported by the Korea Evaluation Institute of Industrial Technology (KEIT) and the Ministry of Trade, Industry & Energy (MOTIE) of the Republic of Korea (20017477). This work was also supported by the Gachon University research fund of 2023(GCU-202400930001).

References

[1] K. Kang, Y. S. Meng, J. Breger, C. P. Grey, and G. Ceder, *Science*, **2006**, *311*, 977–980.
[2] J. B. Goodenough and Y. Kim, *Chem. Mater.*, **2010**, *22(3)*, 587–603.
[3] J. B. Goodenough and K.-S. Park, *J. Am. Chem. Soc.*, **2013**, *135(4)*, 1167–1176.
[4] C. Uhlmann, J. Illig, M. Ender, R. Schuster, and E. Ivers-Tiffée, *J. Power Sources*, **2015**, *279*, 428–438.
[5] W. Cai, C. Yan, Y.-X. Yao, L. Xu, X.-R. Chen, J.-Q. Huang, and Q. Zhang, *Angew. Chem. Int. Ed.*, **2021**, *60(23)*, 13007–13012.

[6] Y. Chen, Y. Kang, Y. Zhao, L. Wang, J. Liu, Y. Li, Z. Liang, X. He, X. Li, N. Tavajohi, and B. Li, *J. Energy Chem.*, **2021**, *59(8)*, 83–99.
[7] P. Poizot, S. Laruelle, S. Grugeon, L. Dupont, and J.-M. Tarascon, *Nature*, **2000**, *407*, 496–499.
[8] A. S. Arico, P. Bruce, B. Scrosati, J.-M. Tarascon, and W. van Schalkwijk, *Nat. Mater.*, **2005**, *4*, 366–377.
[9] M. Zheng, H. Tang, L. Li, Q. Hu, L. Zhang, H. Xue, and H. Pang, *Adv. Sci.*, **2018**, *5(3)*, 1700592.
[10] S. Fang, D. Bresser, and S. Passerini, *Adv. Energy Mater.*, **2020**, *10(1)*, 1902485.
[11] K. Ullah, N. Shah, R. Wadood, B. M. Khan, and W. C. Oh, *Nano Trends*, **2023**, *1*, 100004.
[12] O. B. Chae, J. Kim, I. Park, H. Jeong, J. H. Ku, J. H. Ryu, K. Kang, and S. M. Oh, *Chem. Mater.*, **2014**, *26(20)*, 5874–5881.
[13] O. B. Chae, M. Wu, J. B. Lee, J. Jang, J. Kim, J. Y. Kim, W.-B. Jung, S. Lee, J. H. Ryu, and S. M. Oh, *Electrochim. Acta*, **2021**, *398*, 139358.
[14] S. Paul, M. A. Rahman, M. S. Islam, M. R. Islam, and S.-E.-T. Siddiqui, *Battery Energy*, **2022**, *1(4)*, 20220018.
[15] Z. Ren, Q. Chen, X. An, Q. Liu, L. Xie, J. Zhang, W. Yao, M. S. Hamdy, Q. Kong, and X. Sun, *Inorg. Chem.*, **2022**, *61(32)*, 12895–12902.
[16] Q. Wei, X. Chang, D. Butts, R. DeBlock, K. Lan, J. Li, D. Chao, D.-L. Peng, and B. Dunn, *Nat. Commun.*, **2023**, *14*, 7.
[17] X. Li, Y. Tang, L. Liu, Y. Zhang, Y. Gao, M. Qian, and W. Ma, *Nano Res.*, **2024**, *17*, 253–261.
[18] P. Díaz-Carrasco, A. Duarte-Cárdenas, A. Kuhn, and F. García-Alvarado, *J. Power Sources*, **2021**, *515*, 230632.
[19] H. Usui, Y. Domi, T. H. Nguyen, Y. Sadamori, T. Tanaka, and H. Sakaguchi, *ACS Appl. Eng. Mater.*, **2023**, *1(3)*, 994–1000.
[20] A. Zhou, Y. Liu, X. Zhu, X. Li, J. Yue, X. Ma, L. Gu, Y.-S. Hu, H. Li, X. Huang, L. Chen, and L. Suo, *Energy Storage Mater.*, **2021**, *42*, 438–444.
[21] Z. Zhou, R. Yang, Y. Teng, Y. Li, and M. Wei, *J. Colloid Interface Sci.*, **2023**, *637*, 533–540.
[22] N. Kitchamsetti, R. S. Kalubarme, P. R. Chikate, C.-J. Park, Y.-R. Ma, P. M. Shirage, and R. S. Devan, *ChemistrySelect*, **2019**, *4(21)*, 6620–6626.
[23] C. Liu, J. Qian, Y. Ye, H. Zhou, C.-J. Sun, C. Sheehan, Z. Zhang, G. Wan, Y.-S. Liu, J. Guo, S. Li, H. Shin, S. Hwang, T. B. Gunnoe, W. A. Goddard, and S. Zhang, *Nat. Catal.*, **2021**, *4*, 36–45.
[24]W. Zhao, W. Choi, and W.-S. Yoon, *J. Electrochem. Sci. Technol.*, **2020**, *11(3)*, 195–219.
[25] D. P. Opra, S. V. Gnedenkov, and S. L. Sinebryukhov, *J. Power Sources*, **2019**, *442*, 227225.
[26] H. Lindstrom, S. Sodergren, A. Solbrand, H. Rensmo, J. Hjelm, A. Hagfeldt, and S.-E. Lindquist, *J. Phys. Chem. B*, **1997**, *101(39)*, 7710–7716.
[27] K. Liang, X. Chen, Z. Guo, T. Hou, X. Zhang, and Y. Li, *Phys. Chem. Chem. Phys.*, **2016**, *18(35)*, 24370–24376.
[28] G. Liu, M. Huang, Z. Zhang, B. Xi, H. Li, and S. Xiong, *J. Energy Chem.*, **2021**, *53*, 175–184.
[29] L. Thirugnanam, M. Palanisamy, S. Kaveri, S. Ramaprabhu, V. G. Pol, and M. Dutta, *Int. J. Hydrogen Energy.*, **2021**, *46(2)*, 2464–2478.
[30] J. Zhao, D. Wei, X. Zhang, S. Zhang, C. Zhang, and X. Yang, *J. Colloid Interface Sci.*, **2022**, *606*, 577–587.
[31] J. Gao, G. Qiu, H. Li, M. Li, C. Li, L. Qian, and B. Yang, *Electrochim. Acta*, **2020**, *329*, 135175.
[32] D. P. Opra, S. V. Gnedenkov, S. L. Sinebryukhov, A. B. Podgorbunsky, A. A. Sokolov, A. Y. Ustinov, V. G. Kuryavyi, V. Y. Mayorov, and V. V. Zheleznov, *Chem. Phys.*, **2020**, *538*, 110864.
[33] W. H. Choi, C. H. Lee, H. Kim, S. U. Lee, and J. H. Bang, *Nano Energy*, **2020**, *74*, 104829.
[34] Q. He, Z. Sun, X. Shi, W. Wu, J. Cheng, R. Zhuo, Z. Zhang, and J. Wang, *Energy Fuels*, **2021**, *35(3)*, 2717–2726.
[35] Y. Qu, S. Zhu, X. Dong, H. Huang, and M. Qi, *J. Alloys Compd.*, **2021**, *889*, 161612.
[36] U. Alli, K. McCarthy, I.-A. Baragau, N. P. Power, D. J. Morgan, S. Dunn, S. Killian, T. Kennedy, and S. Kellici, *Chem. Eng. J.*, **2022**, *430*, 132976.
[37] C. Xu, S. Zheng, J. Guo, D. Sun, Z. Zhang, and J. Li, *Chem. Eng. J.*, **2023**, *463*, 142295.
[38] W. Zhang, N. Luo, S. Huang, N.-L. Wu, and M. Wei, *ACS Appl. Energy Mater.*, **2019**, *2(5)*, 3791–3797.
[39] B. Li, W. Zhao, Z. Yang, C. Zhang, F. Dang, Y. Liu, F. Jin, and X. Chen, *J. Power Sources*, **2020**, *466*, 228339.
[40] X. Lv, Z. Deng, M. Wang, and J. Deng, *J. Alloys Compd.*, **2022**, *918*, 165697.
[41] Z. H. Mahmoud, Y. Ajaj, G. K. Ghadir, H. M. Al-Tmimi, H. H. Jasim, M. Al-Salih, M. H. S. Alubiady, A. M. Al-Ani, S. S. Jumaa, S. Azat, G. F. Smaisim, and E. Kianfar, *Results Chem.*, **2024**, *7*, 101422.
[42] M. Ni, D. Sun, X. Zhu, Q. Xia, Y. Zhao, L. Xue, J. Wu, C. Qiu, Q. Guo, Z. Shi, X. Liu, G. Wang, and H. Xia, *Small*, **2020**, *16(50)*, 2006366.
[43] L. Li, J. Zhang, Y. Zou, W. Jiang, W. Lei, and Z. Ma, *J. Electroanal. Chem.*, **2019**, *833*, 573–579.
[44] G. Liu, L. Wang, H. G. Yang, H.-M. Cheng, and G. Q. Lu, *J. Mater. Chem.*, **2010**, *20(5)*, 831–843.
[45] G. Liu, L.-C. Yin, J. Wang, P. Niu, C. Zhen, Y. Xie, and H.-M. Cheng, *Energy Environ. Sci.*, **2012**, *5(11)*, 9603.
[46] H. Han, T. Song, J.-Y. Bae, L. F. Nazar, H. Kim, and U. Paik, *Energy Environ. Sci.*, **2011**, *4(11)*, 4532–4536.
[47] G. D. Moon, J. B. Joo, M. Dahl, H. Jung, and Y. Yin, *Adv. Funct. Mater.*, **2014**, *24(6)*, 848–856.
[48] D. Kim, S. Park, J. Mun, and J. H. Ryu, *Int. J. Energy Res.*, **2020**, *44(11)*, 9233–9239.
[49] J. Jang, T. H. Kim, and J. H. Ryu, *Sci. Rep.*, **2021**, *11*, 13095.
[50] P. M. Schaber, J. Colson, S. Higgins, D. Thielen, B. Anspach, and J. Brauer, *Thermochim. Acta*, **2004**, *424(1–2)*, 131–142.
[51] Z. D. Wang, M. Yoshida, and B. George, *Comput.*

Theor. Chem., **2013**, *1017*, 91–98.
[52] K. S. Park, A. Benayad, D.-J. Kang, and S.-G. Doo, *J. Am. Chem. Soc.*, **2008**, *130(45)*, 14930–14931.
[53] D. Mitoraj and H. Kisch, *Chem. - Eur. J.*, **2010**, *16(1)*, 261–269.
[54] L. K. Randeniya, A. B. Murphy, and I. C. Plumb, *J. Mater. Sci.*, **2008**, *43*, 1389–1399.
[55] X. Ma, J.-L. Tian, F. Zhao, J. Yang, and B.-F. Wang, *Ionics*, **2018**, *24*, 3771–3779.
[56] W. Song, H. Zhao, L. Wang, S. Liu, and Z. Li, *ChemElectroChem*, **2018**, *5(2)*, 316–321.
[57] R. Asahi, T. Morikawa, T. Ohwaki, K. Aoki, and Y. Taga, *Science*, **2001**, *293(5528)*, 269–271.
[58] J.-Y. Shin, D. Samuelis, and J. Maier, *Adv. Funct. Mater.*, **2011**, *21(18)*, 3464–3472.
[59] S. Y. Huang, L. Kavan, I. Exnar, and M. Gratzel, *J. Electrochem. Soc.*, **1995**, *142(9)*, L142–L144.
[60] A. Stashans, S. Lunell, R. Bergstrom, A. Hagfeldt, and S.-E. Lindquist, *Phys. Rev. B*, **1996**, *53(1)*, 159–170.
[61] M. Sathish, R. P. Viswanath, and C. S. Gopinath, *J. Nanosci. Nanotechnol.*, **2009**, *9(1)*, 423–432.
[62] W. Jiao, N. Li, L. Wang, L. Wen, F. Li, G. Liu, and H.-M. Cheng, *Chem. Commun.*, **2013**, *49(33)*, 3461–3463.